Proceedings of the 3rd IASME/WSEAS Int. Conf. on FLUID DYNAMICS & AERODYNAMICS, Corfu, Greece, August 20-22, 2005 (pp174-179)

A Two-dimension Computational Investigation of the Flow over a Wall-mounted Parabolic Body

PSYCHOUDAKI S.P., LASKOS V.N and FRAGOS V.P.
Department of Hydraulics, Soil Science and Agricultural Engineering
Aristotle University of Thessaloniki, 541 24 Thessaloniki, GREECE
papoutsi@agro.auth.gr
http://www.auth.gr/agro.eb/hydraul/intex.htm

Abstract: - The Galerkin finite element method is used to calculate the Navier-Stokes and continuity equations to study the flow over a parabolic body, in a wind tunnel, at Reynolds numbers from 10 to 700. The Reynolds numbers were calculated with respect to the height of the body and the inlet free stream velocity. The flow is steady and is nominated to be 2D, while the width of body extends to the whole width of the tunnel. The calculated velocity components, streamlines, pressure, vorticity, boundary layer, shear stress and friction coefficient are presented and discussed with the work of other researchers.

Key-Words: Navier-Stokes equations, finite elements, surface mounted bodies.

1 Introduction

This paper studies a nominated 2D flow in a wind tunnel with a parabolic wall-mounted body. The flow is steady and laminar at the inlet. The fluid is Newtonian and incompressible. The Reynolds numbers $(Re)_h$ are calculated with respect to the body's height and the inlet free stream velocity, varying from 10 to 700. The Reynolds numbers calculated with respect to the tunnel's height are equal to eight times $(Re)_h$. The span-wise width of the body is equal to the channel's width.

The flow over a wall-mounted body of different sizes and shapes, even as backward-facing steps, has been investigated by many researchers because the flow has many applications to very important engineering problems. The flow, so far, has been investigated experimentally [1, 2, 9 et al.] and numerically [3, 4, 5, 6, 7, et al.] and it still keeps investigators interest. We first start investigating a 2D flow over a rectangular wall-mounted obstacle [4, 5] using the finite element method to solve Navier-Stokes equations numerically. Since we needed to address other related flow configurations, the air flow over a parabolic body is investigated in the present work. The idea of this work was to predict the intermediate flow over a parabolic mounted body by advancing from a Stokes flow to higher Reynolds numbers and studying the influence of the body to the flow. The body is submerged into the viscous layer of the flow [3] and it is to be seen if the body is disturbing the stream-wise velocity profiles.

2 Governing Equations

The nominated two-dimensional steady air flow around a surface-mounted body is described by the Navier-Stokes and continuity equations in a wind tunnel.

$$(\vec{\nabla}\vec{V})\vec{V} = -\vec{\nabla}p + \frac{1}{\mathrm{Re}}\nu\vec{\nabla}^2\vec{V} \qquad (1)$$

$$\vec{\nabla}\vec{V} = 0 \qquad (2)$$

The computational domain of the flow and the boundary conditions are shown in Fig. 1. The equations and the boundary conditions are non-dimensionalized by the inlet free stream velocity and the body's height. The height of the body is smaller than its width, (h<b).

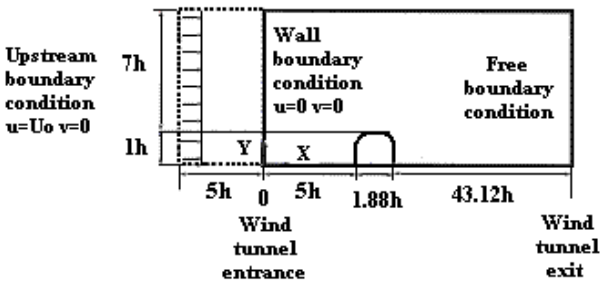

Figure 1. Computational domain of nominally two dimensional flow over a mounted parabolic body

The inlet boundary condition imposes a uniform free stream at the entrance of the computational domain. The no-slip boundary condition is governing along the top and bottom walls of the tunnel and along the surface of the body. The free boundary condition has been applied

at the outflow for a freely flow exit from the computational domain [8].

2.1 Finite Element Formulation

The governing equations (1) and (2) were solved using the finite element (Galerkin) method. The computational mesh is shown in Fig.2. The mesh consists of isoparametric triangle elements with a curved side around the parabola and isoparametric quadrangle elements for the computations further of the parabola.

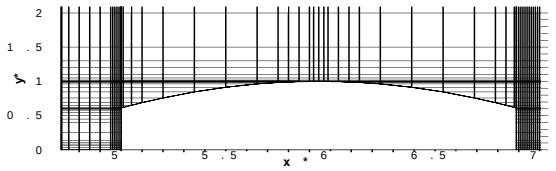

Figure 2. Mesh tessellation of computational domain ,details around the body

The height of the computational domain, eight times the body's height (H=8h), is chosen large enough so that the influence of the boundary conditions on the upper wall shear stress can be weak. The unknown velocities, u and v, were formulated by a quadratic basis function and the pressure, p, by a linear basis. The unknowns were expanded in terms of Galerkin basis functions and weighted integrally with the basis functions taking the following continuity, R_c^i, and momentum, R_M^i, residuals:

$$\mathrm{R}_{\mathrm{c}}^{\mathrm{i}} = \int_{\forall} \vec{\nabla}\vec{\mathrm{V}}\Psi^{\mathrm{i}}\mathrm{d}\forall \qquad (3)$$

$$R_M^i = \int_{\forall} (\vec{V}\vec{\nabla})\vec{V} - \vec{\nabla}(-pI + \frac{1}{\mathrm{Re}}T)\Phi^i d\forall \qquad (4)$$

where $\vec{V}$ is the vector of the velocity, I is the identity matrix, $T = \nabla\vec{V} + (\nabla\vec{V})^T$ is the stress tensor of the Newtonian fluid with $\nabla^2\vec{V} = \nabla T$, $d\forall$ is the infinitely small volume of calculating domain and Ψ^i, Φ^i, are the linear and quadric basic functions in equations (3) and (4) respectively.

Applying the divergence theorem, the order of differentiation equation decreases (4).The residuals are evaluated numerically using nine-point Gaussian integration for the quadrangle elements and six-point Gaussian integration for the triangle ones. The result is a system of nonlinear algebraic equations, which are solved with the Newton-Raphson iterative method. The banded matrix of the resulting linear equation is solved by a frontal solver at each iteration [4, 8]. The program was created by the authors for this work using a VISUAL FORTRAN language.

Table 1

Number of elements	9958
Number of nodes	40311
Number of unknowns	90833
Computer used	Pentium (R) 4 CPU 3.4 GHz 1.00 GB
CPU time per iteration	5.899min
Criterion of convergence	10^{-6} for velocity,$4x10^{-3}$ for pressure
Grid system	$0.005<\Delta x<0.5$, $0.00013<\Delta y<0.25$

3 Results and Discussion

The calculated streamlines for three different Reynolds numbers, 200, 500 and 700, are shown in Figs. 3a, b, c. Fig. 3a shows the region upstream of the mounted body and Fig. 3b shows the region downstream of it. Fig. 3c shows a qualitative comparison of the present work with that of Leone et al. [7] for $(\mathrm{Re})_h = 200$.

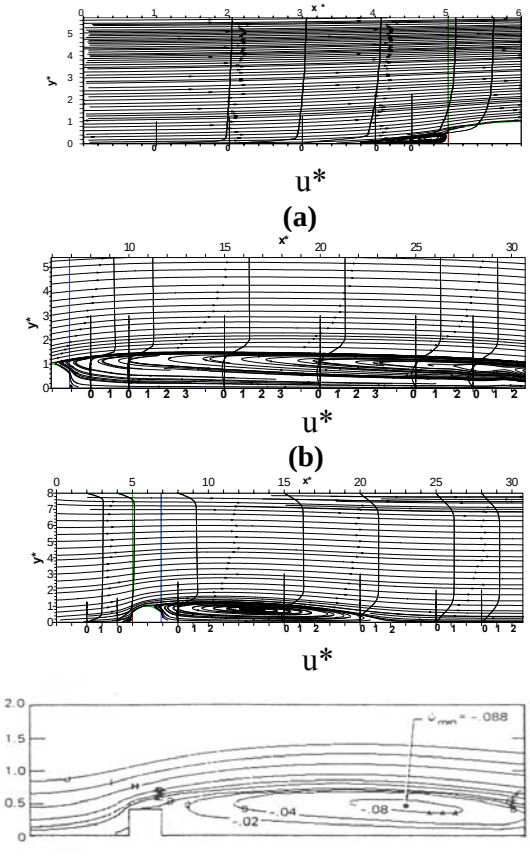

Figures 3a,b,c.Computed streamlines and velocity profiles at different Reynolds numbers,
(a) upstream, (b) downstream of the body, for $(\mathrm{Re})_h$=700, (c) qualitative comparison between the present work and that of Leone et al. [7] for $(\mathrm{Re})_h$=200

Although the similarities are obvious, the present work shows much more details of the flow around the body. It should be noticed that in both flow configurations the separation of the downstream of the bodies recirculation is on the top of the bodies. The investigation of Leone et al. [7] had to do with obtaining accurate solutions of the Navier-Stokes equations with centered finite differences via successive mesh refinement. The better details shown in Fig 3c are owed to much more improved method of solution, number of elements, equations, CPU time and probably the finer mesh. The stream-wise velocity distribution, at different positions along x^*-axes, is also shown in the above figures. In the velocity distributions, in the recirculation regions upstream and downstream of the body, the negative values of the velocities are shown, too.

Comparison of the stream-wise velocity profiles between the present work and that of Fragos et al. [4] are shown in Fig. 4 at different positions along the x^*-axes and the top of the body for $(Re)_h$ = 500. The velocity profiles show an absolute agreement. The difference of the two flow configuration is the size and the shape of the obstacle. In Fragos et al. [4] work the top of the body is horizontally flat and the length equal to the height. In the present work the top is a parabola and the length is longer than the height.

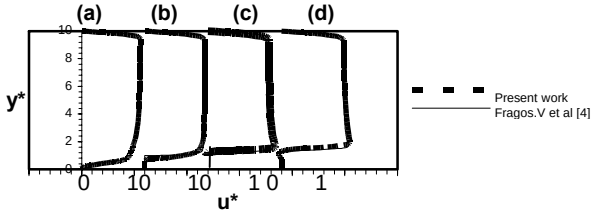

Figure 4. Comparison of longitudinal velocity profiles, (a) in the separation zone, (c) in the middle of the body and the (b) leading and (d) trailing edges of the body

The computed length of separation and reattachment of the present work, compared to computed data of other works, [2, 3, 5, 6] are shown in Figs 5a,b. The experimental data of Acrivos et al. [1], Boum et al. [3] of Armaly et al. with Denham and Patric (1974) [2] and Hong et al. [6] are shown, too, in Fig. 5b.

Figure 6 shows the growth of boundary layer along the x^*-axis for different Reynolds numbers. It is shown that the body is submerged in the shear layer zone. The growth of the boundary layer is decreasing as the Re is increasing, close to the body,

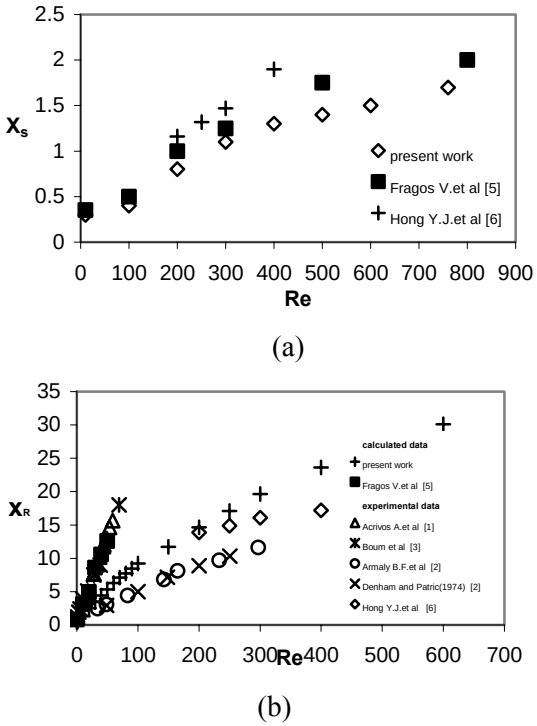

Figure 5a,b. (a) separation and (b) reattachment length upstream and downstream of the body respectively.Comparison of the present work to numerical [3,4,6] and experimental [1,2,6] work

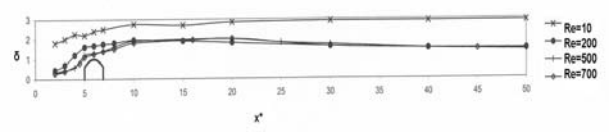

Figure 6. Boundary layer growth along x*-axis for different $(Re)_h$.

to become almost constant downstream of the body, for $(Re)_h$=200,500 and 700.

Figures 7a, b show the stream-wise velocity profiles, in wall coordinates, at two different positions along x^*-axis and for five different Reynolds numbers. The calculation of shear-stress velocity u^* at x^*=2 is based on a flow in the wind-tunnel without the body, while at x^*=45 it is based on the numerically calculated wall shear stress. Figures 7a,b show velocity profiles in normal scales, upstream of separation (x^*=2) and far downstream of reattachment (x*=45). Both figures show that either upstream of separation or downstream of reattachment the boundary layer does not follow a standard linear or logarithmic distribution. It seams that the boundary layer upstream of separation does not develop a normal boundary layer, because the body does not give space to the flow to develop it. Downstream of reattachment it seams that the distance of x=38.12h (x^*=45) downstream of the

body is not enough for a normal boundary layer to develop. Figures 7a,b show also the best fit linear and logarithmic equations of the boundary layer upstream of separation, x^*=2 and downstream of reattachment, x^*=45 for $(Re)_h$=10 to 700.

(a)

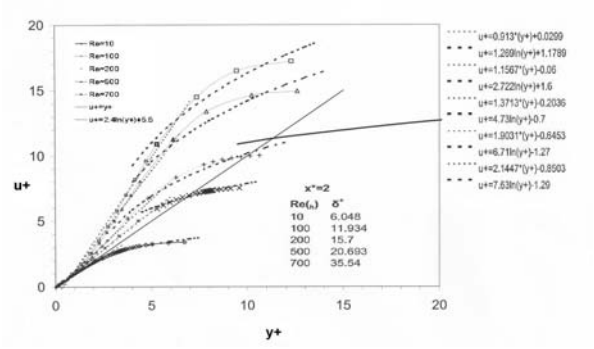

(b)

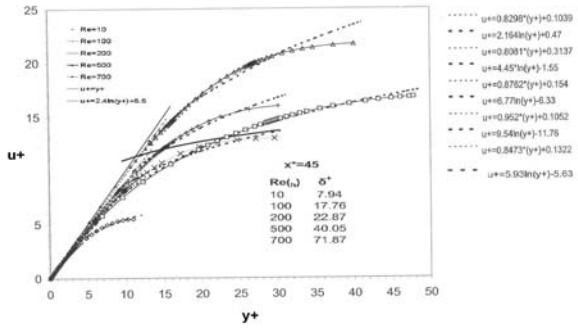

Figures 7 a,b. Distribution of stream-wise velocity and wall terms in linear plot, at two positions. (a) upstream of the body, x*=2 and (b) downstream of reattachment, x*=45, for 10<=Re<=700

Figures 8a, b show a qualitative comparison of the isobars for $(Re)_h$=200 (a) of the present work and that of (b) Leone et al. [7]. The two figures show similar distribution of the isobars around the body. The present work shows more details around the body.

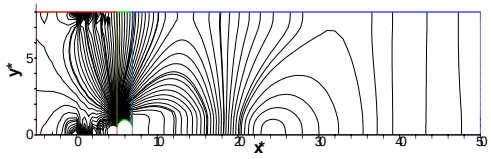

(a)

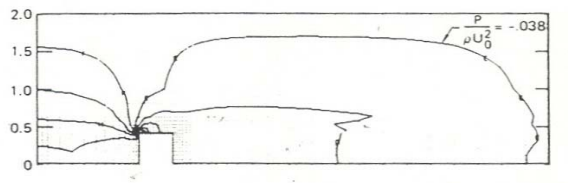

(b)

Figures 8a,b.Qualitative comparison of the isobars for $(Re)_h$=200 of (a) the present work and (b) Leone et al.[7]

Figures 9a,b show qualitative comparison of the pressure coefficient, given by $C_p = 2\Delta p / \rho U_o^2$, along the wall for low Reynolds numbers, between (a) the calculated values of the present work and (b) the experimental data of Acrivos et al. [1].

(a)

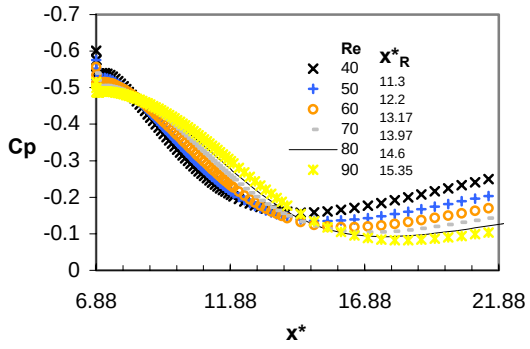

(b)

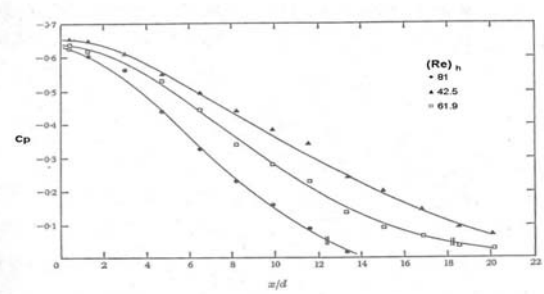

Figures 9a,b.Qualitative comparison of the pressure coefficient along the wall for low Reynolds numbers for (a) the calculated data of present work and (b) for the experimental data of Acrivos et al. [1]

The results of Figs. 9a, b plotted in terms of X/Re=(x^*-6)/Re (for the present work), along the wall downstream of the body are presented in Figs. 10a,b. The qualitative comparison shows an agreement up to x*=14, Fig.9a and X/Re=0.2, Fig. 10a. It should be noticed that the flow configuration of Acrivos et al. is a step while in the present work it is a wall-mounted body.

Figure 11 shows the pressure coefficient variations for $100 \le (Re)_h \le 700$ downstream of the body. It should be noticed that after reattachment the pressure coefficient becomes almost constant.

Figure 12 shows contours of vorticity of the flow domain for two different Reynolds numbers (10, 700). It is clearly shown that the presence of the body in the flow, even at Reynolds number much less than 1000, disturbs the flow far downstream of the body (x=43h) and far higher than the middle of the tunnel's height (y=4h).

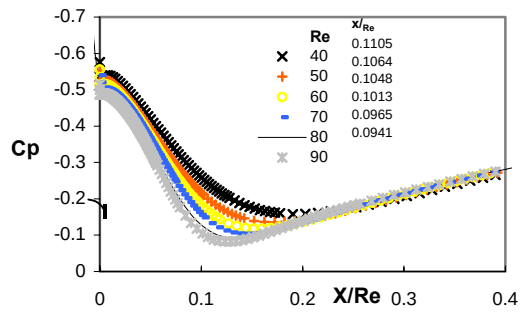

(a)

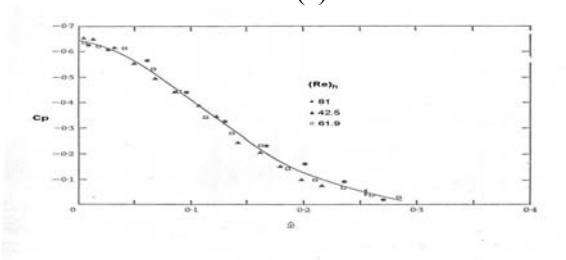

(b)

Figures 10a,b.Qualitative comparison of pressure coefficient in terms of X/Re for low $(Re)_h$ of (a) the calculated data of the present work and (b) the experimental data of Acrivos et al [1]

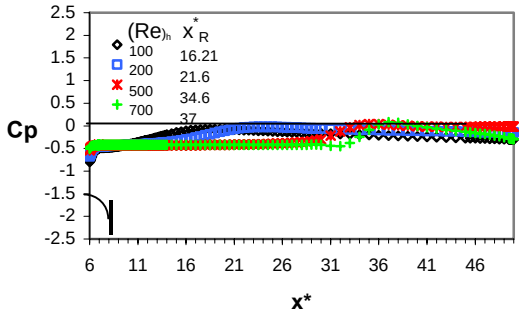

.

Figure 11.Pressure coefficient variations for 100<Re<700 downstream of the body

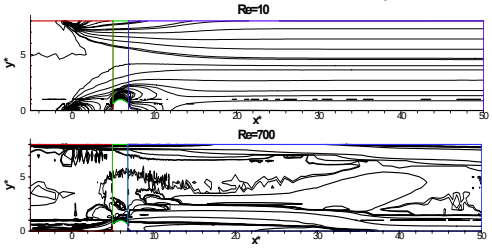

Figure 12.Computed vorticity contours at different Reynolds numbers

The contours of shear stress at two different Reynolds numbers are shown in Fig.13. They show how the shear stress becomes an important feature in the flow because of the body, as the Reynolds number is increasing, although it is between 80<$(Re)_H$<5600, (in tunnel's height). The wall shear stress coefficient expressed as $C_\tau = (\mathrm{Re})_h \tau_w / \rho U_o^2$ (for qualitative comparison), is presented in Figs. 14a, b for low Reynolds numbers.

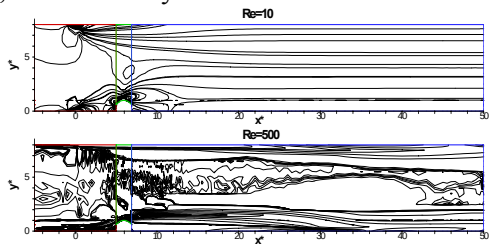

Figure 13. Computed shear stress contours at different Reynolds numbers

Figure 14a shows the distribution of C_τ along x^*-axis of the present work and Fig. 14b shows that of Boum et al. [2]. Apart from the disturbances caused by the inlet conditions and the size of the pick (which in Boum's figure has the double size of that in the present work), both figures show similar distributions, such as a pick on the top of the body, a low downstream of it while far downstream of reattachment the wall shear stress coefficient becomes about equal to one, $C_\tau \approx 1$.

Figure 15 shows the distribution of C_τ for $100 \le (Re)_h \le 700$. It is shown that up to $(Re)_h$ = 200 the distribution is the same as in the previous figures. In the distribution for $(Re)_h$ =500 and 700 the length of x^*=50 seams not enough for the flow to stabilize the wall shear stress to a constant value.

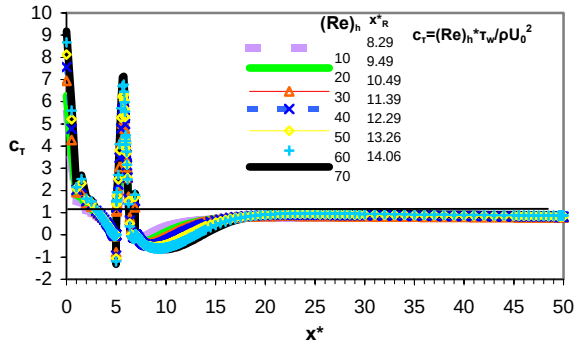

(a)

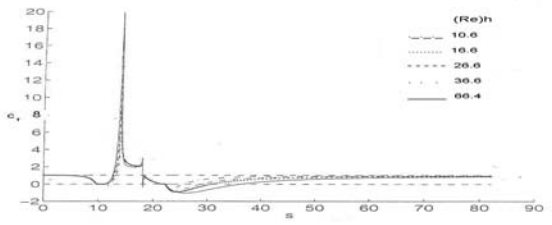

(b)

Figures 14 a,b. Qualitative comparison of wall shear stress coefficient along x*-axis given (a) by the present work and (b) by Boum et al. [3] ,for low Reynolds numbers

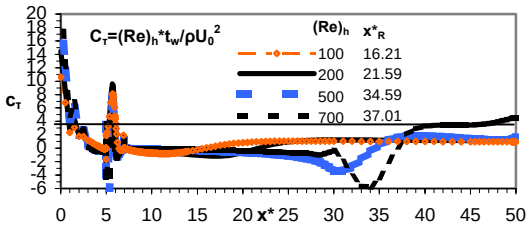

Figure 15.Wall shear stress distribution along x*-axis for 100<$(Re)_h$<700

Conclusions

The Navier-Stokes and continuity equations have been solved numerically, using the finite element method to study a nominally two-dimensional steady flow over a parabolic wall-mounted body for different Reynolds numbers. The Reynolds number is based on body's height and inlet free stream velocity. A uniform free stream flow is applied to the entrance of the tunnel, the no-slip boundary conditions are applied along the walls and the free boundary condition at the exit of the tunnel.

The calculated streamlines show the recirculation regions upstream and downstream of the parabolic body. Qualitative comparison to Leone et al. [7] show very good agreement though the present work shows more details around the body because of the different method of solution (finite elements) and the bigger number of elements, equations, CPU time and the finer mesh. As they suggest, the finite element method "… may be most appropriate if one is seeking accurate solutions ..".

Comparison of the stream-wise velocity distributions of the present work to those of Fragos et al. [4] over a rectangular obstacle, showed a very good agreement. The boundary layer growth for different Reynolds number is higher than the body. The growth of boundary layer is decreasing as the Reynolds number is increasing. The stream-wise velocity profiles, in wall coordinates, show that either upstream of separation or downstream of reattachment the boundary layer does not normally develop, because the flow needs more space upstream and downstream of the body to develop.

Qualitative comparison of the isobars of the present work to the work of Leone et al. [7] and the comparison of the pressure coefficient to the work of Acrivos et al. [1] show very good agreement.

The contours of vorticity show that the presence of the body in the flow disturbs the flow far downstream of the body and far higher than the middle of the tunnel's height. The contours of shear stress also show the influence of the body in the flow. As the Reynold's number is increasing the flow is disturbed up to centre of the tunnel, although $(Re)_H$ is between 80 to 5600. The wall shear stress of the present work compared with that of Boum et al. [3] shows many similarities apart from the disturbances caused by the inlet conditions. Far downstream of reattachment the wall shear stress coefficient becomes about equal to unity for low Reynolds number (up to 200), while for $(Re)_h$ = 500 and 700 it seems that the length of x^* = 50 is not enough for the flow to stabilize the wall shear stress to a constant value.

References

[1] Acrivos A., Leal L.G., Snowden D.D. and Pan F., Further Experiments on Steady Separated Flows Past Bluff Objects, *J. Fluid Mech.,*Vol. 34, Part 1, 1968, pp. 25-48.

[2] Armaly B. F., Durst F., Pereira J. C. F. and oenung B., Experimental and Theoretical Investigation of Backward-facing Step Flow, *J. Fluid Mech.*, Vol. 127, 1983, pp. 473-496.

[3] Boum Ngo G.B., Martemianov S., Alemany A., Computational Study of Laminar Flow and Mass Transfer around a Surface-mounted Obstacle, *Int. J. Heat and Mass Transfer,* Vol. 42, 1999, pp. 2849-2861.

[4] Fragos V.P., Psychoudaki S.P. and Malamataris N.A., Computed-aided Analysis of Flow past a Surface-mounted Obstacle, *Int. J. Num. Methods in Fluids,* Vol. 25, 1997, pp. 495-512.

[5] Fragos V.P., Psychoudaki S.P. and Malamataris N.A., Numerical Experiments of Flow over a Step, *Proc. 2nd Nat. Congress on Computational Mechanics,* Vol. II, Chania, Crete, Greece, 1996, pp. 742-749.

[6] Hong Ying-Jong, Hsieh Shou-Shing and Shih Hnei-Jan, Numerical Computation of Laminar Separation and Reattachment of Flow over Surface mounted Ribs, *Transactions of the ASME, J. Fluids Eng.,* Vol. 113, 1991, pp. 190-198.

[7] Leone J.M. and Gresho P.M., Finite Element Simulations of Steady, Two-dimensional, Viscous, Incompressible Flow over a Step, *J. Compt. Physics,* Vol. 41, 1981, pp. 167-191.

[8] Malamataris N.A., Computed-aided Analysis of Flows on Moving and Unbounded Domains: Phase-change Fronts and Liquid Leveling, *Ph.D. Thesis, Univ. of Mich. Ann Arbor,* 1991.

[9] Martinuzzi R.J. and Abu Omar M., Study of the Flow around Surface-mounted Pyramids, Experiments in Fluids, Experimental Methods and their Applications to Fluid Flow, *10.1007/500348-002-0573-x,* 2004, pp. 1-22.